

Fiber-matrix Contact Stress Analysis for Elastic 2D Composite Solids

Abstract

This paper presents a finite element formulation for the analysis of two dimensional reinforced elastic solids developing both small and large deformations without increasing the number of degrees of freedom. Fibers are spread inside the domain without the necessity of node coincidence. Contact stress analysis is carried out for both straight and curved elements via two different strategies. The first employs consistent differential relations and the second adopts a simple average calculation. The development of all equations is described along the paper. Numerical examples are employed to demonstrate the behavior of the proposed methodology and to compare the contact stress results for both calculations.

Keywords

Finite element method; geometrical nonlinearity; fiber-reinforced solids; contact stress analysis.

Rodrigo Ribeiro Paccola*

Maria do Socorro Martins Sampaio

Humberto Breves Coda

Structural Engineering Department,
Escola de Engenharia de São Carlos,
Universidade de São Paulo

Corresponding author:

*rpaccola@sc.usp.br

<http://dx.doi.org/10.1590/1679-78251282>

Received 11.04.2014

Accepted 21.10.2014

Available online 30.10.2014

1 INTRODUCTION

Composites are made of more than one material in order to take advantage of complementary characteristics. Three widely used composite materials that falls in the fiber reinforced category are the reinforced concrete, the reinforced rubber and the fiber-carbon-epoxy. The reinforced concrete combines the low cost of concrete and its strength to compression with the ductility and strength to traction of the steel. The reinforced rubber combines the large deformability of rubber for dynamic energy absorbing with the steel strength and stiffness. The fiber-carbon composite uses the matrix as a bounding among the carbon fibers. Mechanical analysis of fiber-reinforced composites falls in three main levels: the macro-level, the meso-level and the nano-level. The first is interested in the overall behavior of structural components. The meso-level deals with the interdependent behavior of fiber and matrix, i.e. interfacial stress and slip. Finally the nano-level is interested in the nano-scale constitution of fibers and matrix by themselves and in its influence at meso and macro-levels.

In this paper we intend to collaborate in meso and macro-levels of fiber reinforced modeling via Finite Elements. We propose a way to represent short or long fibers immersed in elastic continuum

domains by means of fiber finite elements without increasing the number of degrees of freedom and a way to calculate, with good precision, the contact stresses (shear and normal) between fiber and matrix without using auxiliary bounding layer strategies.

In FEM literature different ways are developed to incorporate fibers inside matrix domain. The reader is invited to consult the works (Radtke et al., 2011, 2010a, 2010b; Hettich et al., 2008; Chudoba et al., 2009; Oliver et al., 2008) where field enrichments are imposed inside the 2D domain in order to model the fiber-matrix coupling. These enrichments are based on general known behavior of fiber-matrix connections. They are mostly based on the so called Partition of Unity FEM (Melenk and Babuska, 2006; Duarte and Oden, 1996a, 1996b; Oden et al., 1998; Duarte et al., 2000; Babuska and Melenk, 1997). These works are very elegant and well posed; however the pre-known enrichment field is of difficult achievement when, for example, curved fibers are present. Readers are invited to consult the works Schlangen et al. (1992); Bolander and Saito (1997); Liz et al., (2006) in which authors employ lattice strategy to model composites from micro-structures. Moreover, other approaches that adopt slip degrees of freedom to represent the fiber reinforced body can be found in Balakrishnan and Murray (1986); Désir et al. (1999). Works that employ the Boundary Element Method should also be mentioned (Coda, 2001; Leite et al., 2003).

This study presents an alternative geometrically nonlinear formulation to analyze 2D solids reinforced by fibers. The 2D solid finite element applied here to discretize the continuum is isoparametric of any order (Coda, 2009; Coda and Paccola, 2008; Pascon and Coda, 2013). Curved high order fiber elements are developed to be embedded in the continuum. To calculate contact stresses without using slip degrees of freedom two approaches are developed and compared, an average stress calculated from the transfer fiber force resultants and a differential relation among normal fiber internal stress and contact forces. The adopted nodal parameters are positions, not displacements, which is adequate to model curved elements and large deformations due to the natural presence of a numerical chain rule. The formulation is classified as total Lagrangian and the Saint-Venant-Kirchhoff constitutive law is chosen to model the material behavior (Ciarlet, 1993; Ogden, 1984). Therefore, the Green strain and the Second Piola-Kirchhoff stress are adopted.

Fiber elements are introduced in matrix by means of nodal kinematic relations. This strategy directly ensures the adhesion of fibers nodes to the matrix without increasing the number of degrees of freedom and without the need of nodal matching (Sampaio et al., 2013; Vanalli et al., 2008). To solve the resulting geometrical nonlinear problem we adopt the Principle of Stationary Total Potential Energy (Tauchert, 1974). From this principle we find the nonlinear equilibrium equations and the Newton-Raphson iterative procedure (Luenberger, 1989) is used to solve the nonlinear system. External loads are considered conservative and incrementally applied.

The paper is organized as follows. Section 2 describes the general nonlinear solution process, indicating the important variables that will be developed in subsequent sections. Section 3 describes the procedure used to model the two-dimensional continuum. Section 4 presents the developed any order fiber finite element and describes the chain rule applied to generalize the inclusion of fibers into high order 2D solid finite elements without increasing the number of degrees of freedom. Section 5 presents the proposed fiber-matrix contact stresses calculations. Section 6 presents the numerical examples comparing and analyzing the behavior of the proposed formulations. Finally, conclusions are presented in section 7.

2 THE NONLINEAR SOLUTION

In this section, the strategy adopted to solve the reinforced 2D solid geometrically nonlinear equilibrium is described. It is important to clarify that next sections explain how the fiber degrees of freedom are related to the main unknown of the process, i.e., the 2D solid nodal positions without increasing the number of degrees of freedom.

The nonlinear analysis starts writing the total potential energy (Π) as follows:

$$\Pi(Y) = U(Y) + \Omega(Y) \quad (1)$$

where U is the strain energy including matrix and fiber contributions written regarding solid nodal positions and Ω is the potential energy of external conservative applied forces given by:

$$\Omega = -F_j Y_j \quad (2)$$

where F_j is the vector of external forces and Y_j is the current position vector.

The Principle of Stationary Total Potential Energy (Tauchert, 1974) is applied writing the equilibrium equations as the derivative of total energy regarding nodal positions (2D solid for instance), as:

$$g_j = \frac{\partial \Pi}{\partial Y_j} = \frac{\partial U}{\partial Y_j} - F_j = F_j^{\text{int}} - F_j = 0 \quad (3)$$

where F_j^{int} is the internal force vector or the strain energy gradient vector calculated regarding solid nodal positions. The nodal current positions are the unknowns of the problem, so, when adopting a trial position in Eq. (3) g_j is not null and becomes the unbalanced force vector of the Newton-Raphson (Luenberger, 1989) procedure. Expanding the unbalanced force vector around a trial solution \mathbf{Y}^0 , one has:

$$g_j(\mathbf{Y}) = g_j(\mathbf{Y}^0) + \left. \frac{\partial g_j}{\partial Y_k} \right|_{\mathbf{Y}^0} \Delta Y_k + O_j^2 = 0 \quad (4)$$

which can be rewritten, neglecting higher order terms as:

$$\Delta Y_k = - \left(\left. \frac{\partial g_j}{\partial Y_k} \right|_{\mathbf{Y}^0} \right)^{-1} g_j(\mathbf{Y}^0) = - \left(\left. \frac{\partial^2 U}{\partial Y_k \partial Y_j} \right|_{\mathbf{Y}^0} \right)^{-1} g_j(\mathbf{Y}^0) = - (H_{kj})^{-1} g_j(\mathbf{Y}^0) \quad (5)$$

where ΔY_k is the correction of position and $H_{kj} = \partial^2 (U) / \partial (Y_k \partial Y_j) \Big|_{\mathbf{Y}^0}$ is the Hessian matrix or tangent stiffness matrix.

The trial solution is improved by:

$$Y_k = Y_k^0 + \Delta Y_k \quad (6)$$

until ΔY_k or g_j become sufficiently small (Luenberger, 1989). The load level can be incrementally applied if one wants to describe the equilibrium path of the analyzed structure.

3 ISOPARAMETRIC 2D SOLID FINITE ELEMENT – ISOTROPIC CONTINUUM

As we are interested in composite analysis the procedure described in this section is applied to the continuum part of the composite, i.e., the matrix. After achieving the strain energy of the matrix the next section is concerned with the introduction of the fiber strain energy into the mechanical system.

3.1 Kinematical approximation and positional mapping

By means of the illustration of a quadratic finite element, Figure 1 shows the 2D solid (matrix) mapping from the initial configuration (not deformed) B_0 to its current configuration B (Bonet et al., 2000). This mapping is done using a dimensionless auxiliary configuration B_1 .

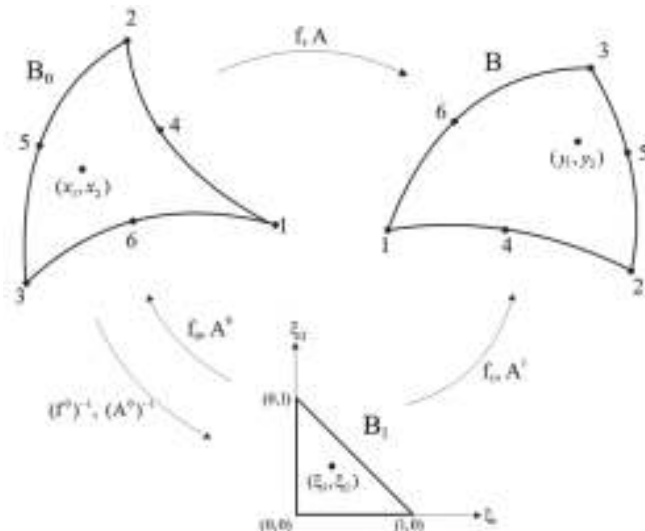


Figure 1: Initial and current configuration mappings.

The initial configuration B_0 whose points have coordinates x_i is mapped from the dimensionless space B_1 with coordinates ξ_i using shape functions of any order, $\phi_l(\xi_1, \xi_2)$, and by the coordinates of the nodes l in the initial configuration, X_i^l , such as:

$$x_i = f_i^0 = \phi_l(\xi_1, \xi_2) X_i^l \quad (7)$$

Similarly, the current configuration B is mapped from the dimensionless space B_1 by the expression:

$$y_i = f_i^1 = \phi_l(\xi_1, \xi_2) Y_i^l \quad (8)$$

where y_i are coordinates of points in the current configuration, Y_i^l are the current node positions, $l = 1, \dots, N$ are nodes and $i = 1, 2$ correspond to coordinate directions.

The deformation function \mathbf{f} that maps the initial configuration B_0 to the current configuration B can be written as a composition of mappings \mathbf{f}^0 and \mathbf{f}^1 as:

$$\mathbf{f} = \mathbf{f}^1 \circ (\mathbf{f}^0)^{-1} \quad (9)$$

The deformation gradient \mathbf{A} can be derived directly from \mathbf{A}^0 and \mathbf{A}^1 as (Bonet et al., 2000; Coda and Paccola, 2007):

$$\mathbf{A} = \mathbf{A}^1 \cdot (\mathbf{A}^0)^{-1}, \text{ with } A_{ij}^0 = \frac{\partial f_i^0}{\partial \xi_j}, A_{ij}^1 = \frac{\partial f_i^1}{\partial \xi_j} \quad (10)$$

Equation (10) can be understood as a numerical chain rule because the initial mapping gradient \mathbf{A}^0 is a known numerical quantity. The solid element has any order of approximation and N is the number of nodes given as a function of the approximation order GP as:

$$N = \frac{(GP + 1)(GP + 2)}{2} \quad (11)$$

3.2 Continuum strain energy

Without loss of generality, to simulate the continuum portion of the composite (matrix) we adopted the Saint-Venant-Kirchhoff specific strain energy function (Ciarlet, 1993; Ogden, 1984), as:

$$u_{mat} = \frac{1}{2} E_{ij} \mathcal{C}_{ijkl} E_{kl} \quad (12)$$

where \mathcal{C}_{ijkl} is the elastic fourth-order tensor and \mathbf{E} is the Green-Lagrange second-order strain expressed respectively by:

$$\mathcal{C}_{ijkl} = \frac{2G\nu}{1-2\nu} \delta_{ij} \delta_{kl} + G (\delta_{ik} \delta_{jl} + \delta_{il} \delta_{jk}) \quad (13)$$

$$E_{ij} = \frac{1}{2} (C_{ij} - \delta_{ij}) = \frac{1}{2} (A_{ki} A_{kj} - \delta_{ij}) \quad (14)$$

The variables $\mathbf{C} = \mathbf{A}^t \cdot \mathbf{A}$ and $\boldsymbol{\delta}$ are the right Cauchy-Green stretch tensor and the Kronecker delta, respectively. In Eq. (13), G is the shear modulus and ν is the Poisson's ratio.

The strain energy accumulated in the continuum part of the composite (matrix) is calculated by integrating the specific strain energy over the initial volume, i.e.,

$$U_{mat} = \int_{V_0} u_{mat} dV_0 \quad (15)$$

Considering solids with unitary thickness and writing Eq. (15) as a function of dimensionless coordinates (ξ_1 and ξ_2) results:

$$U_{mat} = \int_0^1 \int_0^{1-\xi_2} u_{mat}(\xi_1, \xi_2) J_0(\xi_1, \xi_2) d\xi_1 d\xi_2 \quad (16)$$

where J_0 is the Jacobian of the initial mapping, i.e.,

$$J_0(\xi_1, \xi_2) = \det(\mathbf{A}^0) \quad (17)$$

with \mathbf{A}^0 given by Eq. (10).

The matrix strain energy can be derived directly regarding the solid finite element positions finding the conjugate internal force vector, as:

$$F_\alpha^{\beta \text{ int}} = \frac{\partial U_{mat}}{\partial Y_\alpha^\beta} = \int_{V_0} \frac{\partial u_{mat}}{\partial Y_\alpha^\beta} dV_0 = \int_0^1 \int_0^{1-\xi_1} \frac{\partial u_{mat}}{\partial Y_\alpha^\beta} J_0(\xi_1, \xi_2) d\xi_2 d\xi_1 \quad (18)$$

in which α is the direction and β is the node. The derivative inside the integral term of Eq. (18) can be developed as:

$$\frac{\partial u_{mat}}{\partial Y_\alpha^\beta} = \frac{\partial u_{mat}}{\partial \mathbf{E}} : \frac{\partial \mathbf{E}}{\partial \mathbf{C}} : \frac{\partial \mathbf{C}}{\partial Y_\alpha^\beta} = \frac{1}{2} \mathbf{S} : \frac{\partial \mathbf{C}}{\partial Y_\alpha^\beta} \quad (19)$$

where $\mathbf{S} = \partial u_{mat} / \partial \mathbf{E}$ is the second Piola-Kirchhoff stress tensor. From the definition of the right Cauchy stretch and Eq. (10) one writes:

$$\frac{\partial \mathbf{C}}{\partial Y_\alpha^\beta} = (\mathbf{A}^0)^{-T} \cdot \frac{\partial (\mathbf{A}^1)^T}{\partial Y_\alpha^\beta} \cdot \mathbf{A}^1 \cdot (\mathbf{A}^0)^{-1} + (\mathbf{A}^0)^{-T} \cdot (\mathbf{A}^1)^T \cdot \frac{\partial \mathbf{A}^1}{\partial Y_\alpha^\beta} \cdot (\mathbf{A}^0)^{-1} \quad (20)$$

From Eq. (8) results

$$\frac{\partial A_{ij}^1}{\partial Y_\alpha^\beta} = \phi_{l,j}(\xi_1, \xi_2) \frac{\partial Y_i^l}{\partial Y_\alpha^\beta} = \phi_{l,j}(\xi_1, \xi_2) \delta_{\beta l} \delta_{\alpha i} = \phi_{\beta,j}(\xi_1, \xi_2) \delta_{\alpha i} \quad (21)$$

To complete the necessary variables of the solution process (section 2) it is necessary to calculate the second derivative of strain energy regarding nodal positions, resulting into the Hessian matrix as:

$$H_{\alpha\beta\gamma\xi}^{mat} = \frac{\partial^2 U_{mat}}{\partial Y_\alpha^\beta \partial Y_\gamma^\xi} = \int_{V_0} \frac{\partial^2 u_{mat}}{\partial Y_\alpha^\beta \partial Y_\gamma^\xi} dV_0 \quad (22)$$

in which

$$\frac{\partial^2 u_{mat}}{\partial Y_\alpha^\beta \partial Y_\gamma^\xi} = \frac{1}{4} \frac{\partial^2 u_{mat}}{\partial \mathbf{E} \partial \mathbf{E}} : \frac{\partial \mathbf{C}}{\partial Y_\gamma^\xi} : \frac{\partial \mathbf{C}}{\partial Y_\alpha^\beta} + \frac{1}{2} \frac{\partial u_{mat}}{\partial \mathbf{E}} : \frac{\partial^2 \mathbf{C}}{\partial Y_\gamma^\xi \partial Y_\alpha^\beta} \quad (23.a)$$

or

$$\frac{\partial^2 u_{mat}}{\partial Y_\alpha^\beta \partial Y_\gamma^\xi} = \frac{1}{4} \mathbf{c} : \frac{\partial \mathbf{C}}{\partial Y_\gamma^\xi} : \frac{\partial \mathbf{C}}{\partial Y_\alpha^\beta} + \frac{1}{2} \mathbf{S} : \frac{\partial^2 \mathbf{C}}{\partial Y_\gamma^\xi \partial Y_\alpha^\beta} \quad (23.b)$$

and

$$\begin{aligned} \frac{\partial^2 \mathbf{C}}{\partial Y_\alpha^\beta \partial Y_\gamma^\xi} &= (\mathbf{A}^0)^{-T} \cdot \frac{\partial^2 (\mathbf{A}^1)^T}{\partial Y_\alpha^\beta \partial Y_\gamma^\xi} \cdot \mathbf{A}^1 \cdot (\mathbf{A}^0)^{-1} + (\mathbf{A}^0)^{-T} \cdot \frac{\partial (\mathbf{A}^1)^T}{\partial Y_\alpha^\beta} \cdot \frac{\partial \mathbf{A}^1}{\partial Y_\gamma^\xi} \cdot (\mathbf{A}^0)^{-1} + \\ &(\mathbf{A}^0)^{-T} \cdot \frac{\partial (\mathbf{A}^1)^T}{\partial Y_\gamma^\xi} \cdot \frac{\partial \mathbf{A}^1}{\partial Y_\alpha^\beta} \cdot (\mathbf{A}^0)^{-1} + (\mathbf{A}^0)^{-T} \cdot (\mathbf{A}^1)^T \cdot \frac{\partial^2 \mathbf{A}^1}{\partial Y_\alpha^\beta \partial Y_\gamma^\xi} \cdot (\mathbf{A}^0)^{-1} \end{aligned} \quad (24)$$

It should be noted that, for solid elements, the second derivative of \mathbf{A}^1 regarding nodal parameters is null, simplifying expression (24) to:

$$\frac{\partial^2 \mathbf{C}}{\partial Y_\alpha^\beta \partial Y_\gamma^\xi} = (\mathbf{A}^0)^{-T} \cdot \frac{\partial (\mathbf{A}^1)^T}{\partial Y_\alpha^\beta} \cdot \frac{\partial \mathbf{A}^1}{\partial Y_\gamma^\xi} \cdot (\mathbf{A}^0)^{-1} + (\mathbf{A}^0)^{-T} \cdot \frac{\partial (\mathbf{A}^1)^T}{\partial Y_\gamma^\xi} \cdot \frac{\partial \mathbf{A}^1}{\partial Y_\alpha^\beta} \cdot (\mathbf{A}^0)^{-1} \quad (25)$$

Next section presents the necessary expressions to introduce fibers into the composite formulation.

4 ELASTIC FIBER REINFORCEMENT – KINEMATICS AND ENERGY CONSIDERATIONS

This section is divided into two subsections. The first describes the strain energy of general curved fibers and the second describes the strategy used to introduce fiber energy in the composite solution without increasing the number of degrees of freedom.

4.1 Any order curved fiber element

To guaranty total adherent fiber-matrix coupling when using high order solid elements it is also necessary to adopt high order fiber elements (Sampaio et al., 2013). Figure 2 shows the non-deformed initial configuration B_0 , the current configuration B and a non-dimensional auxiliary configuration B_1 for the curved fiber finite element of any order.

The initial configuration B_0 whose points have coordinates x_i is mapped from the dimensionless space B_1 with coordinates ξ using shape functions of any order, $\phi_P(\xi)$, and by the coordinates of nodes P , X_i^P , at the initial configuration, such as:

$$x_i = f_i^0 = \phi_P(\xi) X_i^P \quad (26)$$

The current configuration B is mapped from the dimensionless space B_1 by:

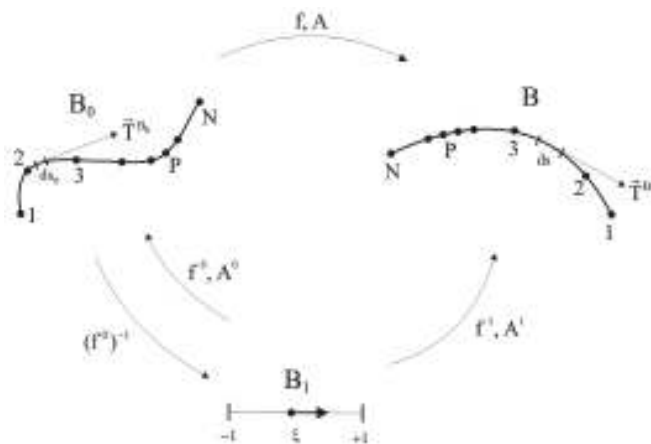


Figure 2: Mapping of the fiber finite element - initial and current configurations.

$$y_i = f_i^1 = \phi_P(\xi) Y_i^P \tag{27}$$

where y_i are the coordinates of points in the current configuration B and Y_i^P are the current coordinates of fiber nodes. In Eqs. (26) and (27) index $P = 1, \dots, N$ and $i = 1, 2$ represent, respectively, the fiber finite element nodes and coordinate directions.

The tangent vector of the fiber and its modulus are calculated at the initial configuration as

$$T_i^{B_0} = \frac{d\phi_P(\xi)}{d\xi} X_i^P \quad \text{and} \quad |\vec{T}^{B_0}|^2 = \left(\frac{d\phi_P(\xi)}{d\xi} X_1^P \right)^2 + \left(\frac{d\phi_P(\xi)}{d\xi} X_2^P \right)^2 \tag{28}$$

It is important to mention that $|\vec{T}^{B_0}|$ is the differential Jacobian of f_i^0 . For the current configuration one finds:

$$T_i^B = \frac{d\phi_P(\xi)}{d\xi} Y_i^P \quad \text{and} \quad |\vec{T}^B|^2 = \left(\frac{d\phi_l(\xi)}{d\xi} Y_1^P \right)^2 + \left(\frac{d\phi_l(\xi)}{d\xi} Y_2^P \right)^2 \tag{29}$$

Using Eqs. (28) and (29) one write the one-dimensional Green strain as

$$E = \frac{1}{2} \left(\frac{|\vec{T}^B|^2 - |\vec{T}^{B_0}|^2}{|\vec{T}^{B_0}|^2} \right) \tag{30}$$

or in its expanded form,

$$E = \frac{1}{2} \frac{\left[\left(\frac{d\phi_l(\xi)}{d\xi} Y_1^P \right)^2 + \left(\frac{d\phi_l(\xi)}{d\xi} Y_2^P \right)^2 \right] - \left[\left(\frac{d\phi_l(\xi)}{d\xi} X_1^P \right)^2 + \left(\frac{d\phi_l(\xi)}{d\xi} X_2^P \right)^2 \right]}{\left(\frac{d\phi_l(\xi)}{d\xi} X_1^P \right)^2 + \left(\frac{d\phi_l(\xi)}{d\xi} X_2^P \right)^2} \tag{31}$$

Using the Saint-Venant-Kirchhoff constitutive law one writes the specific strain energy at a point of the fiber as:

$$u_f(\xi) = \frac{1}{2} \boldsymbol{\epsilon} \cdot [E(\xi)]^2 \quad (32)$$

where $\boldsymbol{\epsilon}$ is the elastic modulus and $E(\xi)$ is the Green strain measure defined by Eq. (30) or (31).

The strain energy of a curved fiber is given by integrating equation (32) over its initial volume V_0 as:

$$U_f = \int_{V_0} u_f dV_0 \quad (33)$$

In order to proceed with the equilibrium analysis it is necessary to know the first derivative of strain energy regarding positions. Based on the energy conjugate concept the natural internal fiber force vector related to node j and direction k ($F_k^{jff\text{int}}$) is calculated regarding fiber parameters as:

$$F_k^{jff\text{int}} = \frac{\partial U_f}{\partial Y_k^j} = \int_{V_0} \frac{\partial u_f}{\partial Y_k^j} dV_0 \quad (34)$$

From Eqs. (31) and (32) follows

$$F_k^{jff\text{int}} = \frac{\partial U_f}{\partial Y_k^j} = \int_{V_0} \boldsymbol{\epsilon} \cdot E \frac{\left(\frac{d\phi_l(\xi)}{d\xi} Y_k^l \right) \frac{d\phi_j(\xi)}{d\xi}}{|T^0|^2} dV_0 = \int_{V_0} E \cdot S dV_0 \quad (35)$$

in which S is the one-dimensional Second Piola-Kirchhoff stress. Considering S constant over the cross section area A of the fiber one transforms dV_0^f into a simple expression, resulting:

$$F_k^{jff\text{int}} = \int_0^{L_0} \boldsymbol{\epsilon} \cdot E \frac{\left(\frac{d\phi_l(\xi)}{d\xi} Y_k^l \right) \frac{d\phi_j(\xi)}{d\xi}}{|T^0|^2} A ds_0 = \int_{-1}^1 \boldsymbol{\epsilon} \cdot E \frac{\left(\frac{d\phi_l(\xi)}{d\xi} Y_k^l \right) \frac{d\phi_j(\xi)}{d\xi}}{|T^0|^2} J_0(\xi) \cdot A d\xi \quad (36)$$

Where, as mentioned before,

$$J_0(\xi) = |\vec{T}^0| = \sqrt{\left(\frac{dx_1}{d\xi} \right)^2 + \left(\frac{dx_2}{d\xi} \right)^2} \quad (37)$$

The Hessian matrix components for the fiber element are obtained by the second derivative of the strain energy, i.e.:

$$H_{kj\alpha\beta}^f = \frac{\partial^2 U_f}{\partial Y_k^j \partial Y_\alpha^\beta} = \int_{V_0^f} \frac{\partial^2 u_f}{\partial Y_k^j \partial Y_\alpha^\beta} dV_0^f = \int_{V_0^f} h_{kj\alpha\beta}^f dV_0^f \quad (38)$$

Developing the necessary calculations one achieves:

$$H_{kj\alpha\beta}^f = \int_{V_0} \left(\frac{\boldsymbol{\epsilon} \cdot \mathbf{E}}{|T^0|^4} \left(\frac{d\phi_l(\xi)}{d\xi} Y_\alpha^l \right) \frac{d\phi_\beta(\xi)}{d\xi} \left(\frac{d\phi_l(\xi)}{d\xi} Y_k^l \right) \frac{d\phi_j(\xi)}{d\xi} + \frac{\boldsymbol{\epsilon} \cdot \mathbf{E}}{|T^0|^2} \frac{d\phi_\beta(\xi)}{d\xi} \frac{d\phi_j(\xi)}{d\xi} \delta_{k\alpha} \right) dV_0 \quad (39)$$

or

$$H_{kj\alpha\beta}^f = \int_{-1}^1 \left(\frac{\boldsymbol{\epsilon} \cdot \mathbf{E}}{|T^0|^4} \left(\frac{d\phi_l(\xi)}{d\xi} Y_\alpha^l \right) \frac{d\phi_\beta(\xi)}{d\xi} \left(\frac{d\phi_l(\xi)}{d\xi} Y_k^l \right) \frac{d\phi_j(\xi)}{d\xi} + \frac{\boldsymbol{\epsilon} \cdot \mathbf{E}}{|T^0|^2} \frac{d\phi_\beta(\xi)}{d\xi} \frac{d\phi_j(\xi)}{d\xi} \delta_{k\alpha} \right) A \cdot J_0(\xi) d\xi \quad (40)$$

Integrals (36) and (40) are solved using Gauss-Legendre quadrature.

The parameters used to find the internal force and Hessian matrix for fibers are not suitable to be directly applied in the solid solution process; in next section the necessary transformations are presented.

4.2 Coupling strategy – kinematical fiber matrix coupling

The procedure adopted here to embed fibers at any position of the domain without increasing the number of degrees of freedom is an extension of the works of Vanalli et al. (2008) where linear elements and linear elasticity were adopted.

4.2.1 General fiber / solid connection

The requisite to start the procedure to embed curved fibers in curved solid elements is to know the solid dimensionless coordinates related to fiber nodes coordinates. This is done solving the pair of dimensionless solid variable (ξ_1^p, ξ_2^p) associated to the physical fiber node position in the following nonlinear system,

$$\phi_l(\xi_1^p, \xi_2^p) X_i^l = X_i^p \quad (41)$$

where ϕ_l are the shape functions of the solid element, X_i^p are the known physical coordinates of fiber nodes (generated independently of solid mesh) and X_i^l are the know solid nodes coordinates. To solve Eq. (41) one expands it in Taylor series until the first order and starts with a trial dimensionless coordinate, (ξ_1^{pt}, ξ_2^{pt}) , i.e.:

$$X_i^p \cong \phi_l(\xi_1^{pt}, \xi_2^{pt}) X_i^l + \left. \frac{\partial \phi_l(\xi_1, \xi_2)}{\partial \xi_j} \right|_{(\xi_1^{pt}, \xi_2^{pt})} \Delta \xi_j \quad \text{or} \quad X_i^p = X_i^{Pt} + H_{ij} \Delta \xi_j \quad (42)$$

in which X_i^{Pt} is a trial position of the fiber node calculated from the solid element geometry and the trial dimensionless coordinates and H_{ij} is a two dimensional matrix. The correction of the trial dimensionless coordinates $\Delta\xi_i$ is calculated solving the following linear system of equation:

$$H_{ij}\Delta\xi_j = X_i^P - X_i^{Pt} \quad (43)$$

The procedure is a simple and fast Newton-Raphson nonlinear solver that relates all fiber nodes to the connected solid element revealing the pair of dimensionless variables (ξ_1^P, ξ_2^P) . From this information one also knows the current position of fiber nodes as a function of solid nodes positions, i.e.,

$$Y_i^P = \phi_l(\xi_1^P, \xi_2^P)Y_i^l \quad (44)$$

in which Y_i^l are the current positions of solid nodes. Equation (44) ensures the connection among nodes of fibers and the matrix 2D elements.

In the next item it will be necessary to differentiate the fiber strain energy regarding the solid nodal coordinates using the chain rule. To make it possible one has to differentiate Eq. (44) regarding a generic nodal solid coordinate, as:

$$\frac{\partial Y_i^P}{\partial Y_\alpha^\beta} = \frac{\partial Y_i^l}{\partial Y_\alpha^\beta} \phi_l(\xi_1^P, \xi_2^P) = \delta_{\alpha i} \delta_{\beta l} \phi_l(\xi_1^P, \xi_2^P) \quad (45)$$

If the fiber node P belongs to the solid element then $\delta_{\beta l} = 1$ and if direction α (solid) is equal to direction i (fiber) then $\delta_{\alpha i} = 1$ and expression (45) results $\partial Y_i^P / \partial Y_\alpha^\beta = \phi_\beta(\xi_1^P, \xi_2^P)$, otherwise it results zero.

4.2.2 General internal force

The strain energy stored in a reinforced body is the sum of the strain energies stored in the matrix and fibers,

$$U = U_{mat} + U_f \quad (46)$$

where U_{mat} is the strain energy stored in the 2D solid finite elements used to discretize the matrix and U_f is the strain energy stored in the fiber finite elements. Therefore, the internal force at a node β following direction α , considering both fiber and matrix contributions is found by the conjugate energy concept, such as:

$$\frac{\partial(U_{mat} + U_f)}{\partial Y_\alpha^\beta} = \frac{\partial U_{mat}}{\partial Y_\alpha^\beta} + \frac{\partial U_f}{\partial Y_\alpha^\beta} = \frac{\partial U_{mat}}{\partial Y_\alpha^\beta} + \frac{\partial U_f}{\partial Y_i^P} \frac{\partial Y_i^P}{\partial Y_\alpha^\beta} = F_\alpha^{\beta mat} + \phi_\beta(\xi_1^P, \xi_2^P) F_\alpha^{Pf} = F_\alpha^{\beta int} \quad (47)$$

where Eqs. (18), (36) and (45) have been used and there is no summation over P .

4.2.3 Hessian Matrix

Proceeding as described for the calculation of internal forces, we develop the second derivative of strain energy of the reinforced finite element regarding the solid nodal parameters, as follows

$$\frac{\partial^2 U}{\partial Y_\alpha^\beta \partial Y_\gamma^\xi} = \frac{\partial^2 (U_{mat} + U_f)}{\partial Y_\alpha^\beta \partial Y_\gamma^\xi} = \int_{V_0} \frac{\partial^2 (u_{mat} + u_f)}{\partial Y_\alpha^\beta \partial Y_\gamma^\xi} dV_0 = \int_{V_0} \frac{\partial^2 u_{mat}}{\partial Y_\alpha^\beta \partial Y_\gamma^\xi} dV_0 + \int_{V_0^f} \frac{\partial^2 u_f}{\partial Y_\alpha^\beta \partial Y_\gamma^\xi} dV_0^f \quad (48)$$

The first integral at the last term of Eq. (48) is known, Eq. (22). However, it is necessary to observe that the kernel of the last integral is the specific strain energy of a fiber derived twice regarding the solid nodal parameters. As Eq. (39) gives its value when derived regarding fiber parameters one has to apply the chain rule twice, described by Eq. (45), over Eq. (48), that is:

$$\frac{\partial^2 u_f}{\partial Y_\alpha^\beta \partial Y_\gamma^\xi} = \frac{\partial^2 u_f}{\partial Y_\omega^\rho \partial Y_\omega^\rho} \frac{\partial Y_\omega^\rho}{\partial Y_\alpha^\beta} \frac{\partial Y_\omega^\rho}{\partial Y_\gamma^\xi} + \frac{\partial^2 u_f}{\partial Y_\omega^\rho \partial Y_\pi^\eta} \frac{\partial Y_\omega^\rho}{\partial Y_\alpha^\beta} \frac{\partial Y_\pi^\eta}{\partial Y_\gamma^\xi} + \frac{\partial^2 u_f}{\partial Y_\pi^\eta \partial Y_\omega^\rho} \frac{\partial Y_\pi^\eta}{\partial Y_\alpha^\beta} \frac{\partial Y_\omega^\rho}{\partial Y_\gamma^\xi} + \frac{\partial^2 u_f}{\partial Y_\pi^\eta \partial Y_\pi^\eta} \frac{\partial Y_\pi^\eta}{\partial Y_\alpha^\beta} \frac{\partial Y_\pi^\eta}{\partial Y_\gamma^\xi} \quad (49)$$

$$\frac{\partial^2 u_f}{\partial Y_\alpha^\beta \partial Y_\gamma^\xi} = h_{\omega\rho\omega\rho}^f \frac{\partial Y_\omega^\rho}{\partial Y_\alpha^\beta} \frac{\partial Y_\omega^\rho}{\partial Y_\gamma^\xi} + h_{\omega\rho\pi\eta}^f \frac{\partial Y_\omega^\rho}{\partial Y_\alpha^\beta} \frac{\partial Y_\pi^\eta}{\partial Y_\gamma^\xi} + h_{\pi\eta\omega\rho}^f \frac{\partial Y_\pi^\eta}{\partial Y_\alpha^\beta} \frac{\partial Y_\omega^\rho}{\partial Y_\gamma^\xi} + h_{\pi\eta\pi\eta}^f \frac{\partial Y_\pi^\eta}{\partial Y_\alpha^\beta} \frac{\partial Y_\pi^\eta}{\partial Y_\gamma^\xi} \quad (50)$$

where h^f is the fiber Hessian matrix kernel, Eq. (38). In Eq. (50) summation is not implied.

Integrating (50) over fiber volume gives:

$$\frac{\partial^2 U_f}{\partial Y_\alpha^\beta \partial Y_\gamma^\xi} = H_{\omega\rho\omega\rho}^f \frac{\partial Y_\omega^\rho}{\partial Y_\alpha^\beta} \frac{\partial Y_\omega^\rho}{\partial Y_\gamma^\xi} + H_{\omega\rho\pi\eta}^f \frac{\partial Y_\omega^\rho}{\partial Y_\alpha^\beta} \frac{\partial Y_\pi^\eta}{\partial Y_\gamma^\xi} + H_{\pi\eta\omega\rho}^f \frac{\partial Y_\pi^\eta}{\partial Y_\alpha^\beta} \frac{\partial Y_\omega^\rho}{\partial Y_\gamma^\xi} + H_{\pi\eta\pi\eta}^f \frac{\partial Y_\pi^\eta}{\partial Y_\alpha^\beta} \frac{\partial Y_\pi^\eta}{\partial Y_\gamma^\xi} \quad (51)$$

Using Eq. (51) into (48) results the consistent spreading of fibers contribution over the matrix properties, i.e.:

$$H = H_{ef} + H_f \quad (52)$$

5 CONTACT STRESS CALCULATION

In the proposed formulation the contact stresses are not used to achieve the equilibrium position. Therefore, the contact stress calculation is done after solving the problem for positions. Two strategies are presented in order to do this calculation. The first is based on differential relations and is presented in subsections 5.1 and 5.2. The second is an average calculation, shown at subsection 5.3, for which the transferred nodal force from fiber to matrix is decomposed following the tangential and normal directions of fiber node and divided by a influence portion of the element contact area.

5.1 Shear contact stress – differential formulation

The differential equilibrium depicted in Figure 3 is used to calculate the contact shear stress $q(\xi)$ between fiber and matrix as:

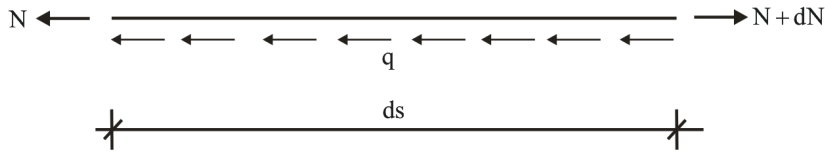


Figure 3: Differential equilibrium following fiber direction.

$$q \cdot t \cdot ds = dN = \frac{dN}{ds} ds \Rightarrow q = \frac{1}{t} \frac{dN}{ds} \quad (53)$$

where ds is a differential of the curvilinear coordinate along the deformed fiber and t is the fiber thickness. ds is calculated as a function of dimensionless coordinate ξ as:

$$ds = \sqrt{dy_1^2 + dy_2^2} = \sqrt{\left(\frac{dy_1}{d\xi} d\xi\right)^2 + \left(\frac{dy_2}{d\xi} d\xi\right)^2} = J(\xi) \cdot d\xi \quad (54)$$

or

$$\frac{ds}{d\xi} = J(\xi) \quad (55)$$

Using the chain rule results:

$$\frac{dN}{ds} = \frac{dN}{d\xi} \cdot \frac{d\xi}{ds} = \frac{dN}{d\xi} \frac{1}{\frac{ds}{d\xi}} = \frac{1}{J(\xi)} \cdot \frac{dN}{d\xi} \quad (56)$$

Considering constant thickness the Cauchy stress is calculated from Piola Kirchhoff stress as:

$$\sigma(\xi) = \frac{J(\xi)}{J_0(\xi)} S(\xi) = \frac{J(\xi)}{J_0(\xi)} \mathcal{E} \cdot E(\xi) \quad (57)$$

$$N(\xi) = \frac{J(\xi)}{J_0(\xi)} \mathcal{E} \cdot E(\xi) \cdot A \quad (58)$$

With $E(\xi)$ given by equation (31).

Instead of differentiate expression (58) regarding ξ and substituting into (56) and (53) we prefer to calculate the normal force nodal values using (31) and (58) and make:

$$N(\xi) = \phi_p(\xi) N^p \quad (59)$$

therefore:

$$\frac{dN}{d\xi}(\xi) = \frac{d\phi_p(\xi)}{d\xi} N^p \quad (60)$$

Substituting (60) into (56) and (56) into (53) results:

$$q(\xi) = \frac{1}{t} \frac{1}{J(\xi)} \frac{d\phi_p(\xi)}{d\xi} N^p \quad (61)$$

It is important to mention that the differential formulation cannot be applied for linear fiber element, as it results null values of $q(\xi)$.

5.2 Normal contact stress – differential formulation

For an infinitesimal length ds there is a curvature center and a curvature radius, see Figure 4. From this figure one writes the following geometrical relation:

$$ds = R.d\theta \quad (62)$$

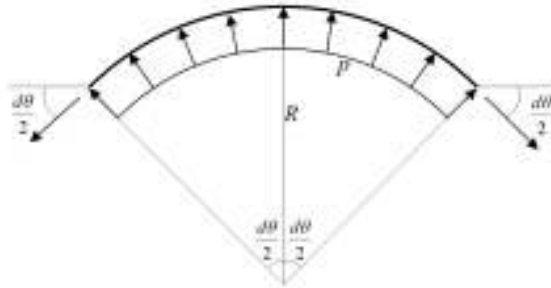


Figure 4: Infinitesimal part of a fiber finite element.

Remembering that t is the body thickness, the equilibrium equation following the fiber orthogonal direction is given by:

$$p.t.ds = p.t.(R.d\theta) = 2.N.\text{sen}\left(\frac{d\theta}{2}\right) = N.d\theta \quad (63)$$

or

$$p(\xi) = \frac{1}{t} \frac{N(\xi)}{R(\xi)} \quad (64)$$

As $N(\xi)$ is known, equation (58), it is necessary to calculate $1/R(\xi)$, given by:

$$\frac{1}{R(\xi)} = \frac{\frac{d^2 y_2}{d\xi^2} \frac{dy_1}{d\xi} - \frac{d^2 y_1}{d\xi^2} \frac{dy_2}{d\xi}}{(J(\xi))^3} \quad (65)$$

Substituting (65) into (64) results the final expression:

$$p(\xi) = \frac{1}{t} N(\xi) \frac{\frac{d^2 y_2}{d\xi^2} \frac{dy_1}{d\xi} - \frac{d^2 y_1}{d\xi^2} \frac{dy_2}{d\xi}}{(J(\xi))^3} \quad (66)$$

By the same reason described in the previous item, expression (66) cannot be applied for linear fiber elements. In section 6 examples are used to demonstrate the use of presented expressions.

5.3 Average contact stress

A generic nodal transfer force (from matrix to fiber) \vec{F}^{int} is depicted in Figure 5 together with the tangential and normal unit vectors (\vec{n} and \vec{t}) calculated at the same point. The tangential and normal components of the transfer force are:

$$\vec{Q} = \vec{F}^{int} \cdot \vec{t} \quad (67)$$

$$\vec{P} = \vec{F}^{int} \cdot \vec{n} \quad (68)$$

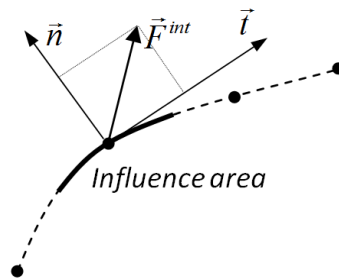


Figure 5: Transfer force and area of influence.

The normal and tangential forces are divided by the surface influence area (A_{inf}) depicted in Figure 5 and the average values results:

$$\vec{q} = \vec{F}^{int} \cdot \vec{t} / A_{inf} \quad (69)$$

$$\vec{p} = \vec{F}^{int} \cdot \vec{n} / A_{inf} \quad (70)$$

It is worth noting that for connecting nodes the resulting value is the average between values calculated for each element.

6 NUMERICAL EXAMPLES

Five numerical examples are chosen to show the behavior of the proposed formulation regarding the overall behavior of reinforced structural members and the estimated contact stress accuracy. A convergence analysis is carried out for both displacement and contact stresses.

6.1 Simple supported beam

This example is used to certify that the mechanical coupling between fiber and matrix is working

properly. Both displacement and contact stress are compared to a simple analytical solution limited to small displacements and strains in order to certify the coherence of results.

It is a simple supported reinforced beam, depicted in Figure 6, subjected to a uniformly distributed load $q = 10 \text{ N/cm}$. The simple supports are modeled by vertical distributed loads of $q_r = 100 \text{ N/cm}$ and the adopted geometrical properties are: $L = 400 \text{ cm}$, $h = 20 \text{ cm}$, $b = 1 \text{ cm}$ and $d = 1 \text{ cm}$, see Figure 6. The Young modulus and the Poisson's ratio of the matrix are $E_c = 21 \times 10^5 \text{ N/cm}^2$ and $\nu = 0$, while the Young modulus and the cross-sectional area of the reinforcement are $E_f = 210 \times 10^5 \text{ N/cm}^2$ and $A_f = 1 \text{ cm}^2$. Due to symmetry, only a half of the problem is solved as depicted by Figure 6.

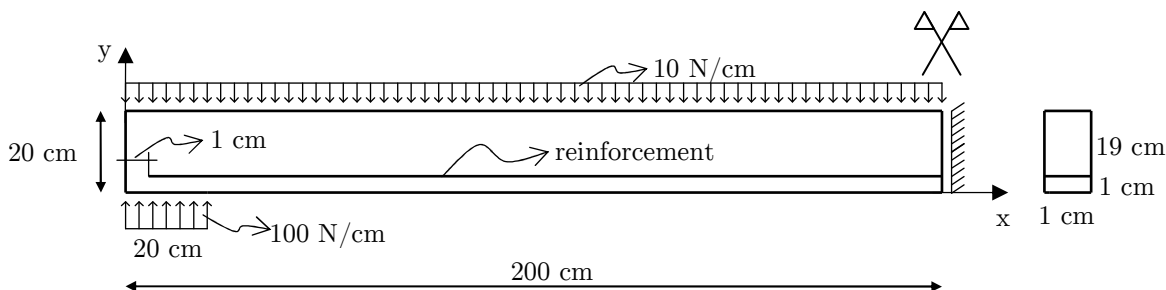


Figure 6: Geometry and boundary conditions.

In order to check displacement convergence, see Figure 7, we use 160 linear fiber elements to discretize the horizontal reinforcement and three different meshes of triangular third order finite elements, i.e., mesh (a) 8×80 elements and 12050 dof, (b) 16×160 elements and 47138 dof and (c) 32×320 elements and 186434 dof. As one can see the displacement difference from the second to the third discretization is less than 0.3% characterizing convergence. Adopting the mid position of reaction as the span position one achieves the technical reference value $q\ell^4 / (384 \cdot EI) = 1.105 \text{ cm}$ obviously smaller than the achieved numerical value.

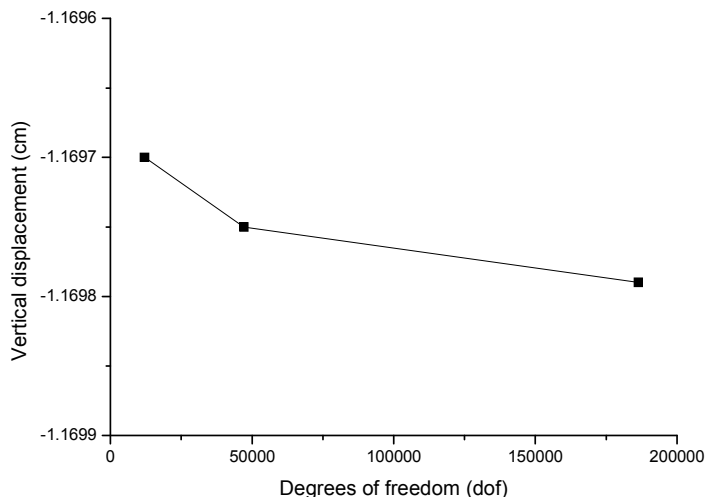


Figure 7: Displacement convergence.

The convergence analysis for shear contact stress is made using linear fibers and the average technique, see Figure 8. We adopt 80 and 160 linear fibers for meshes (a), (b) and (c). As one can see there is no significant difference in results characterizing convergence. However, it is important to note that when one increases the number of fiber finite elements it is also necessary to increase the continuum mesh.

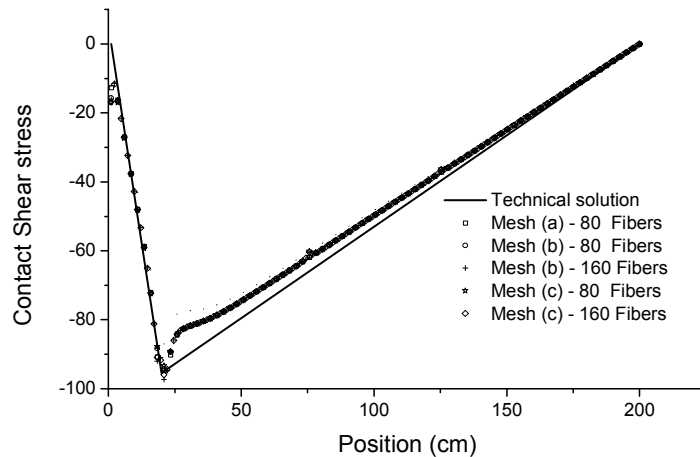


Figure 8: Contact shear stress behavior.

Adopting the average calculation formulation and using mesh (b), Figure 9 compares the shear contact stress for equally spaced nodes using 160 linear, 80 quadratic and 53 third order fiber approximations. Figure 10 shows the same results of Figure 9 when the differential procedure is adopted to calculate the shear stress for second and third order approximations (remembering that the differential procedure is not applied for first order approximation).

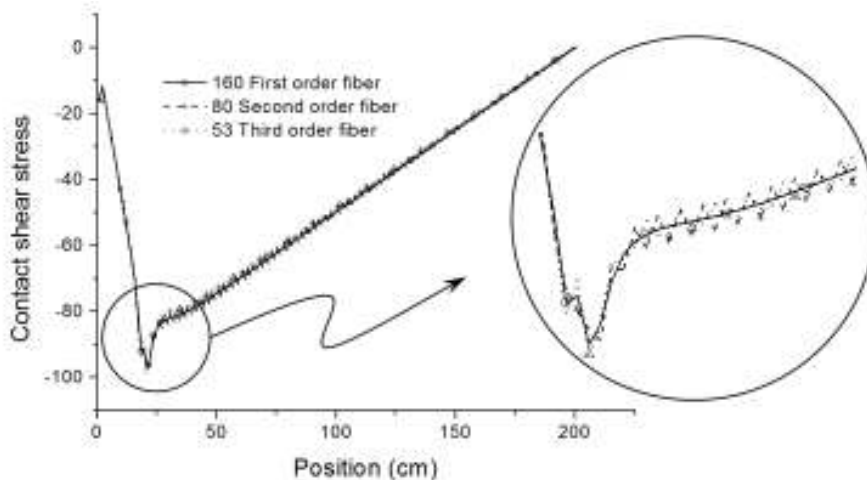


Figure 9: Contact shear stress for high order elements (average calculation).

From Figures 9 and 10 one concludes that when using high order fiber elements a perturbation of the shear contact stress appears; moreover the use of differential formulation, expected to be the

most precise one, introduces even more oscillations. At the beginning we did not know why this spurious behavior appears, however after thinking over the subject we conclude that, due to the nodal characteristic of internal force transfer from matrix to fibers a not recommended finite element operation is taking place.

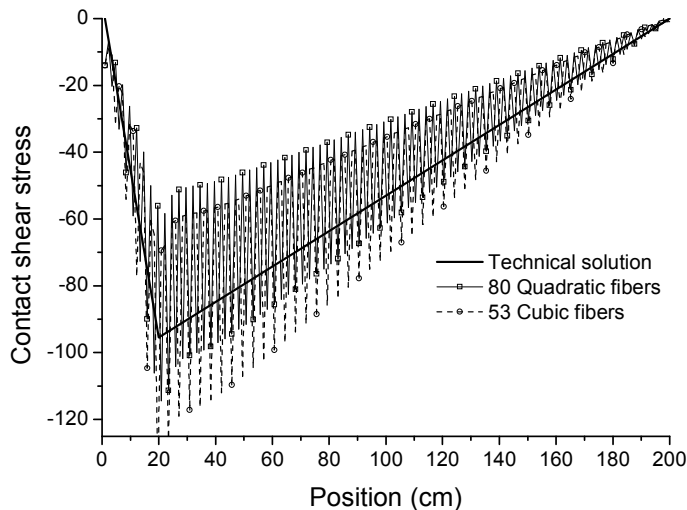


Figure 10: Contact shear stress for high order elements (differential calculation).

This not recommended operation is the application of concentrated forces at central points of higher order finite elements which leads to well-known spurious displacements and stiffness distributions. To illustrate the reason of this perturbation the horizontal displacement of node B of the simple example depicted in Figure 11 is solved using two first order bar finite elements and one second order bar finite element.

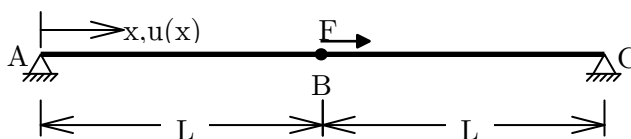


Figure 11: Simple example to reveal the spurious contact shear stress behavior of high order reinforcement finite elements.

Using two linear elements one achieves exactly the analytical result, i.e., $u_B = Fl/(2EA)$, however when using one second order element the result is $u_B = 3Fl/(8EA)$, a wrong solution that reveals the inappropriate force transfer and stiffness distribution of high order fiber elements immersed in the continuum matrix.

Therefore, one concludes that, although achieving a better adherence between fibers and matrix when using high order fiber elements (as demonstrated by Sampaio et al. (2013)) the contact stress distribution is better described by simple linear fiber elements. Moreover, using a good discretization for linear fiber elements an adequate adherence is achieved, see Sampaio et al. (2013).

In order to be complete, Figure 12 shows the stress distribution in the continuum matrix using mesh (c) and 160 linear fiber elements. Figure 13 shows the normal stress along the reinforcement.

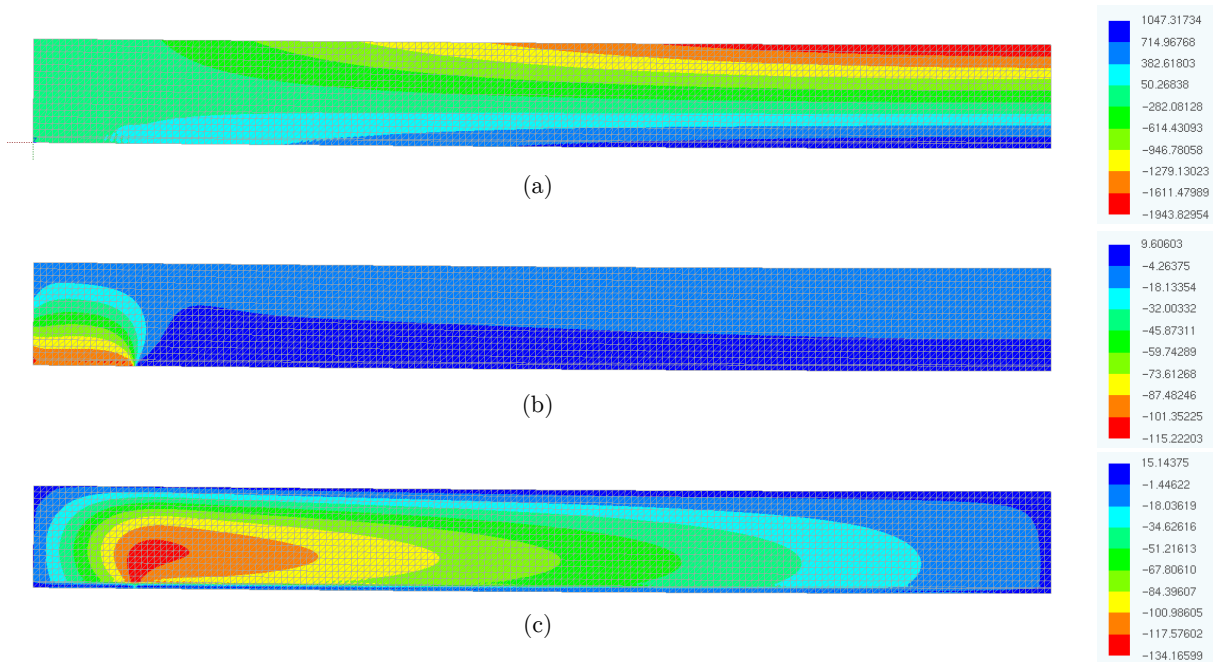


Figure 12: Matrix stress distribution in N/cm^2 , (a) σ_{11} , (b) σ_{22} and (c) σ_{12} .

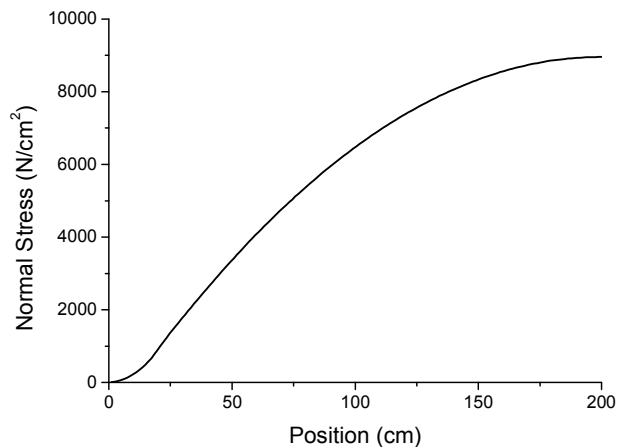


Figure 13: Normal stress along the reinforcement.

6.2 Reinforced ring subjected to a pin force

In this example the reinforced ring of Figure 14a is analyzed. The material properties and cross section are the same used in the previous example. Two values of applied force are employed. The first ($P = 2 \text{ kN}$) is used to compare results with an analytical solution based on Euler-Bernoulli kinematics. The second ($P = 200 \text{ kN}$) is used to show the geometrical non-linear influence in the

developed contact stress. Due to symmetry only a half of the problem is discretized, as depicted in Figure 14b. The adopted matrix mesh (8×240) is chosen after a convergence analysis.

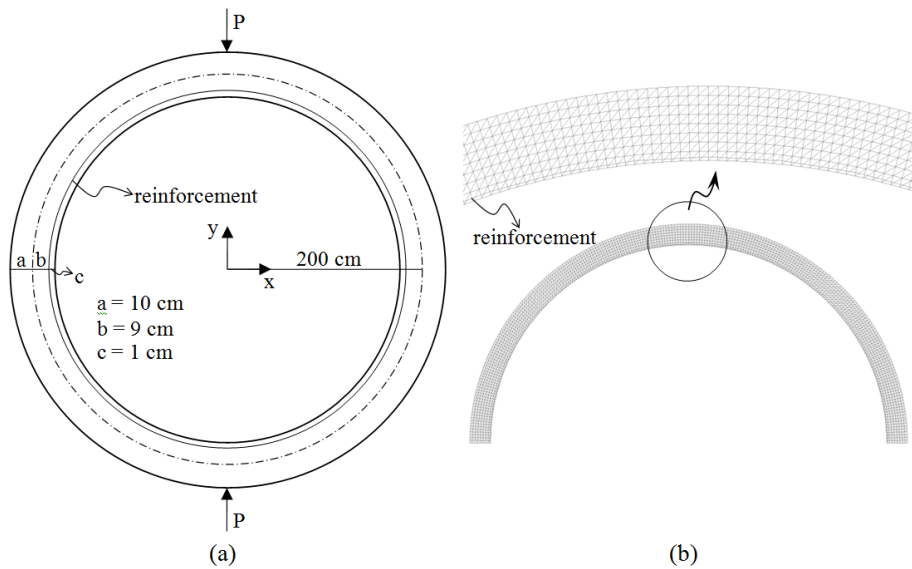


Figure 14: Geometry and matrix discretization.

For $P = 2\text{kN}$ Figure 15 compares the analytical shear stress and the ones achieved using the average technique for 240 and 120 linear fiber elements. Obviously that the analytical solution is only a reference value as the Euler-Bernoulli hypothesis excessively simplifies the problem. In Figure 16 one finds the same result using 240 quadratic and 480 cubic elements, revealing the same spurious behavior detected in the previous example for high order elements. Figure 17 shows the normal contact stress for the same load level using linear fiber elements. As expected the normal contact stress increases near the loaded region.

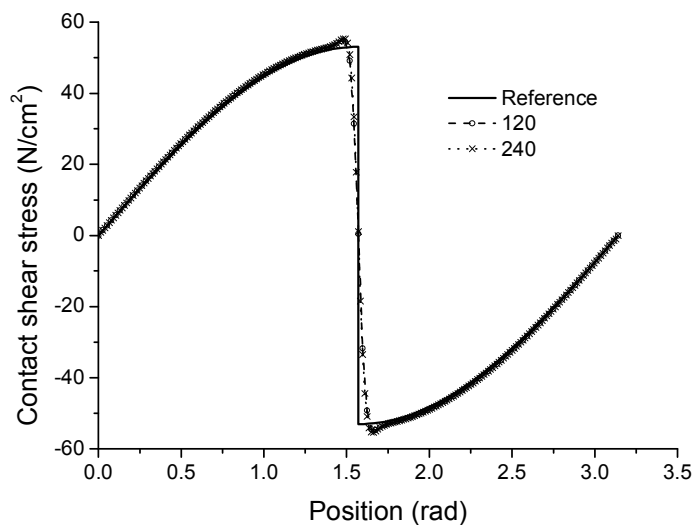


Figure 15: Contact shear stress distribution – Linear elements.

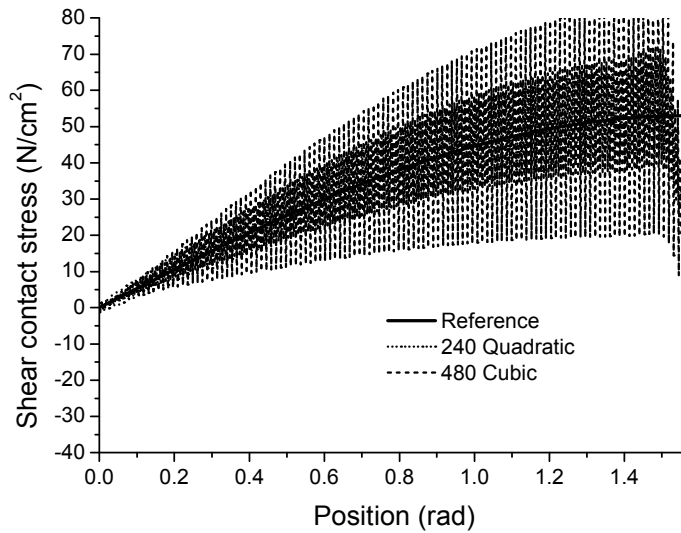


Figure 16: Contact shear stress distribution – High order elements.

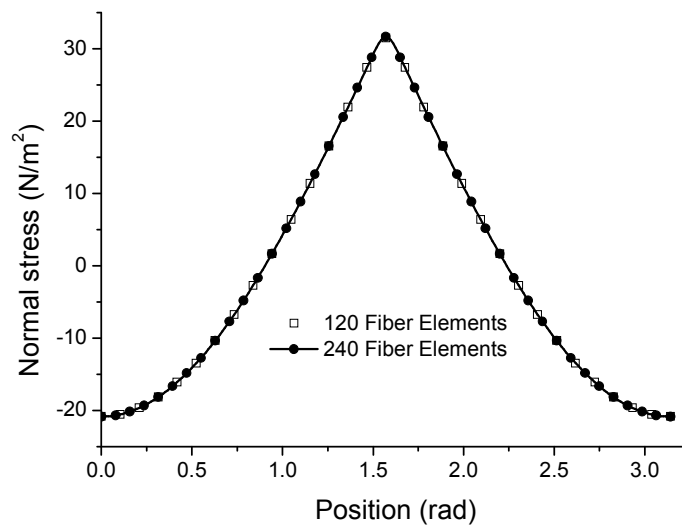


Figure 17: Contact normal stress distribution – Linear elements.

In Figure 18 we multiply by 100 the result of Figure 15 and compare it to the shear contact stress achieved when effectively using $P = 200$ kN. This procedure indicates the influence of large displacements in results. Figure 19 shows the deformed configuration for $P = 200$ kN with the Cauchy stress distribution inside the matrix.

6.3 Curved reinforcement

In this example the same beam modeled in example 1 is solved considering the curved reinforcement as depicted in Figure 20.

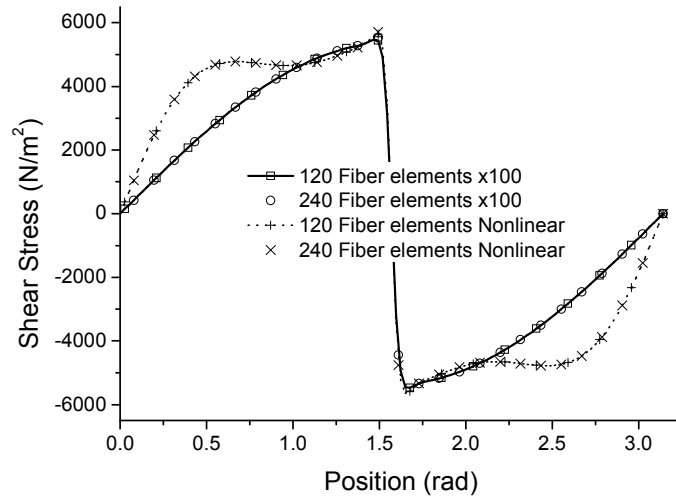


Figure 18: Large displacement influence in contact shear stress distribution.

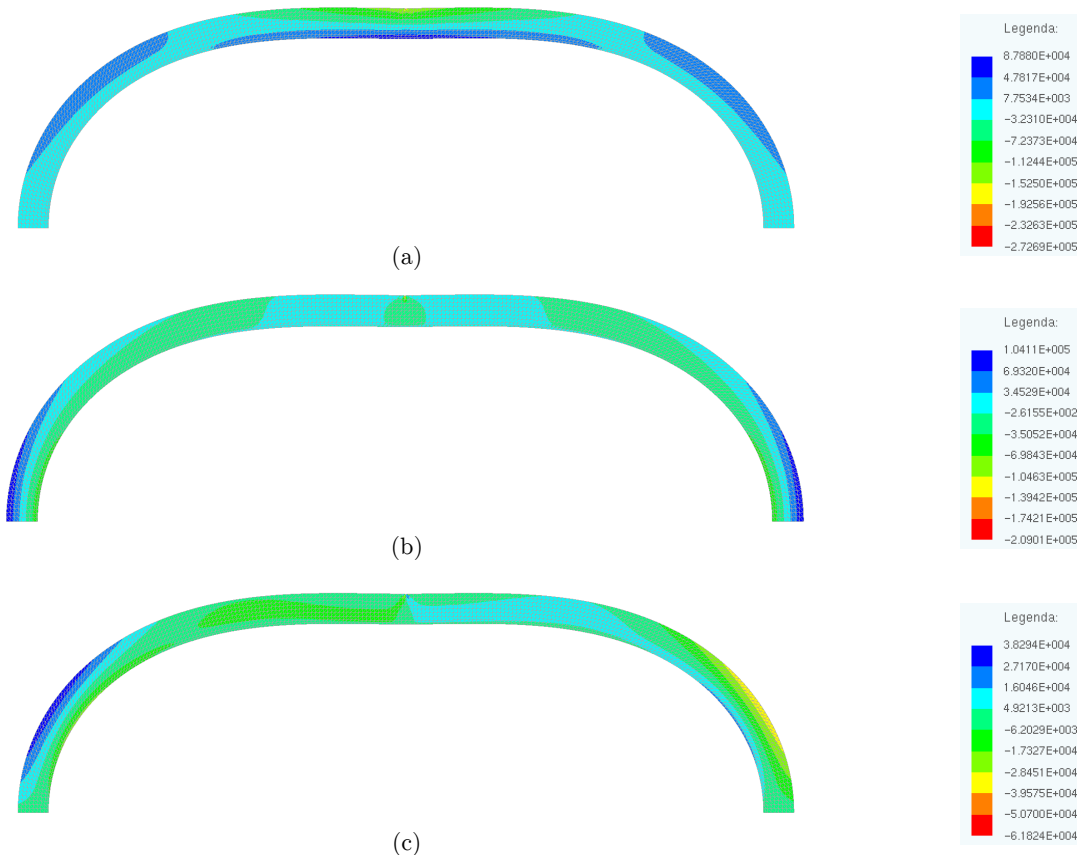


Figure 19: Cauchy stress distribution for $P = 200 \text{ kN}$, (a) σ_{11} , (b) σ_{22} and (c) σ_{12} .

The matrix adopted discretization is mesh (b) 16×160 elements and 47138 dof of example 1. In Figure 21 the horizontal component of the contact stresses is depicted using 155 linear fiber elements along the straight part of the reinforcement and 12 linear fiber elements along the curved

Latin American Journal of Solids and Structures 12 (2015) 583-611

part. These values are compared to the shear contact stress of example 1. The difference in position is obvious as the curved bar is longer than the horizontal one.

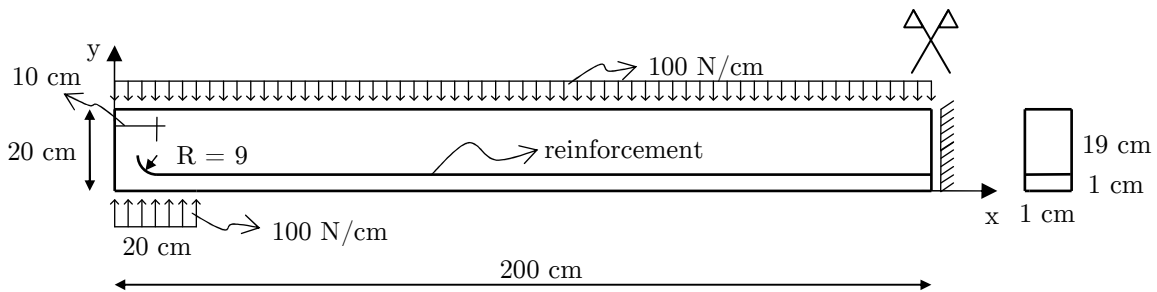


Figure 20: Geometry and reinforcement details.

From this comparison one may note that when using curved reinforcement a faster transfer of the reinforcement normal force to the continuum occurs. Moreover, a change of sign of this transfer appears at the free extremity of the curve, corresponding to a normal contact stress among fiber and matrix, see Figure 22.

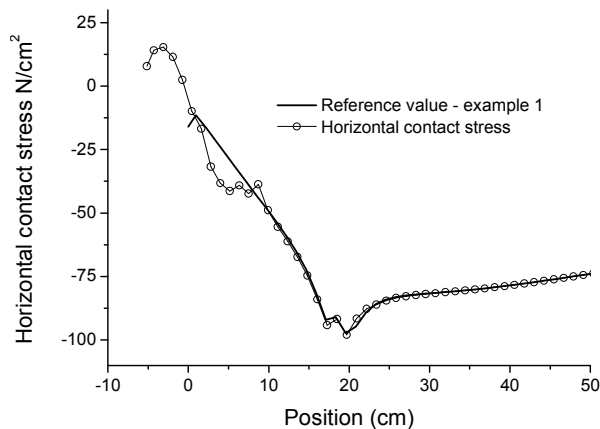


Figure 21: Horizontal component of contact stresses.

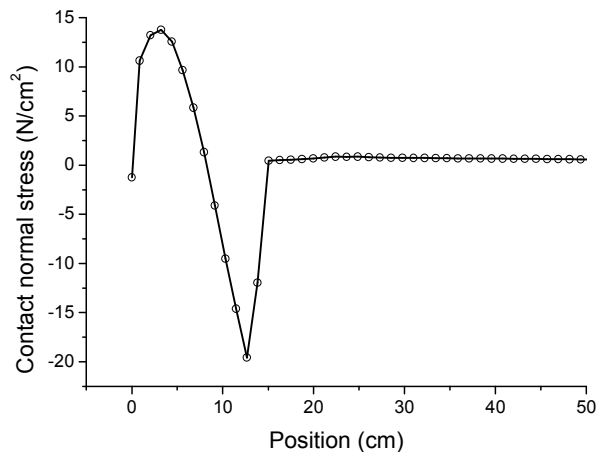


Figure 22: Contact normal stress – curvilinear coordinate.

In Figure 23 the vertical component of the contact stresses is depicted. As it is expected, integrating the area above and under the zero line of this graphic results zero.

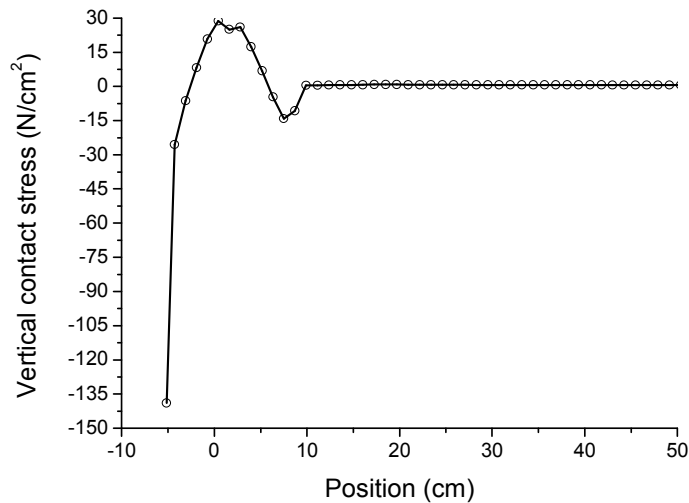


Figure 23: Vertical component of contact stresses.

6.4 Stretch of a reinforced bar (long fiber)

This example is the stretch of a reinforced bar as depicted in Figure 24. The length of the bar is $\ell = 200$ cm, the height is $h = 20$ cm and the thickness is $b = 1$ cm. The reinforcement has area $A = 1$ cm² and is placed at the center of the cross section distant 20 cm from the bar extremities. Due to symmetry a half of the problem is solved, see Figure 24. The matrix property is the same as the adopted in the first example. The reinforcement elastic modulus is varied from $E_m = 210 \times 10^5$ N/cm² to $E_f = 210 \times 10^7$ N/cm². A distributed traction load of 50.000 N/cm² is applied at the extremities.

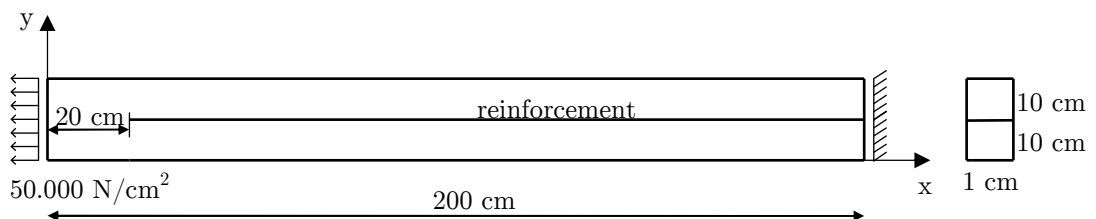


Figure 24: Geometry and boundary conditions.

The adopted matrix discretization is 32×320 , mesh (c) of example 1. In Figure 25 the contact shear stress is evaluated for $E_f = 210 \times 10^5$ N/cm² and using 80, 160 and 320 linear fiber elements. Due to the previous results the average strategy is assumed. As expected the elastic problem is mesh dependent because the shear stress presents unbound value at the extremity of the bar.

Figure 26 shows the maximum displacement of the matrix as a function of the number of fiber elements, the relative difference among the last two values is less than 0.05% which characterizes that overall displacement presents low sensitivity to the discretization of fiber.

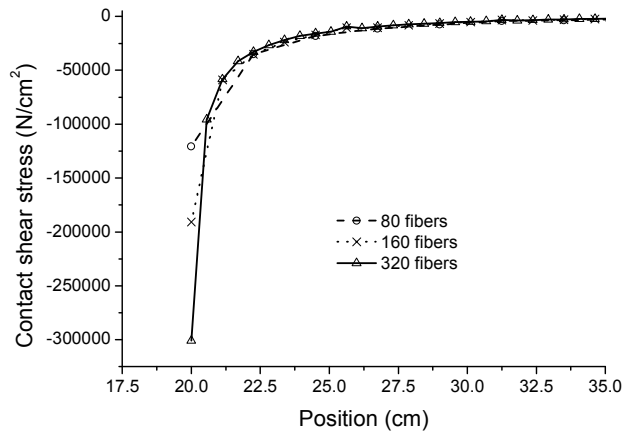


Figure 25: Contact shear stress behavior regarding reinforcement discretization.

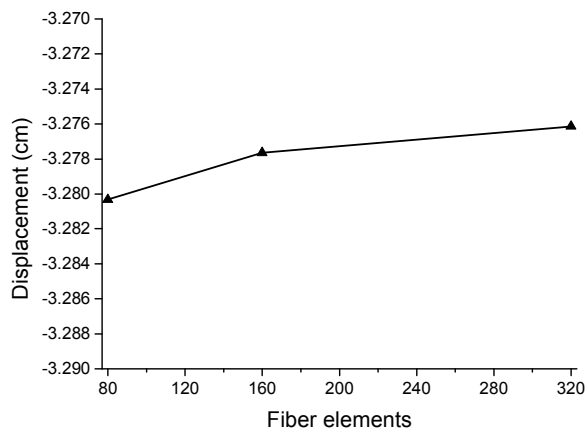


Figure 26: Maximum matrix displacement.

In Figure 27 we present the shear contact stress behavior regarding the elastic modulus of the reinforcement. The behavior of the shear stress does not present a proportionality regarding the stiffness of reinforcement, but becomes more singular, i.e., presents a more pronounced maximum at extremities as the elastic modulus difference between fiber and matrix grows.

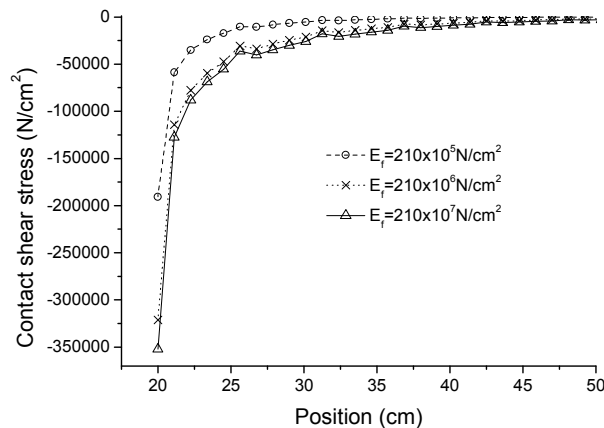


Figure 27: Contact shear stress behavior regarding reinforcement stiffness.

Figure 28 illustrates the reinforcement influence on the matrix σ_{11} stress behavior. Almost all stress is transferred to the bar along less than 25 cm. It is important to mention that the limits adopted in legend of Figure 28 are taken on purpose to show the transition that is hidden if the total stress range is assumed.



Figure 28: Matrix horizontal stress behavior ($E_f = 210 \times 10^7 \text{ N/cm}^2$).

6.5 Stretch of a reinforced bar (short random fibers)

The same bar of example 6.5 is reinforced by 4000 random short fibers instead of a single long fiber. Short fibers are 5 cm long and have a cross section area of 0.1 cm^2 . Three values of elastic modulus are adopted: $E_f = 210 \times 10^6 \text{ N/cm}^2$, $E_f = 210 \times 10^7 \text{ N/cm}^2$ and $E_f = 210 \times 10^8 \text{ N/cm}^2$. The random fibers and the matrix discretization are depicted in Figure 29.

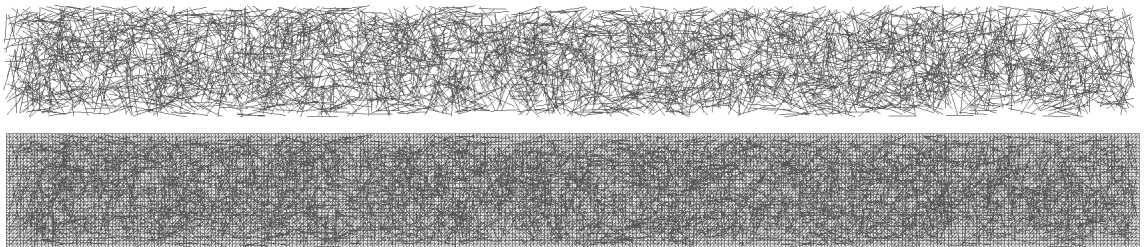


Figure 29: Random fibers and matrix discretization.

The matrix horizontal stress distributions for different fiber elastic modulus are presented in Figure 30. The same maximum and minimum values have been adopted to facilitate comparisons.

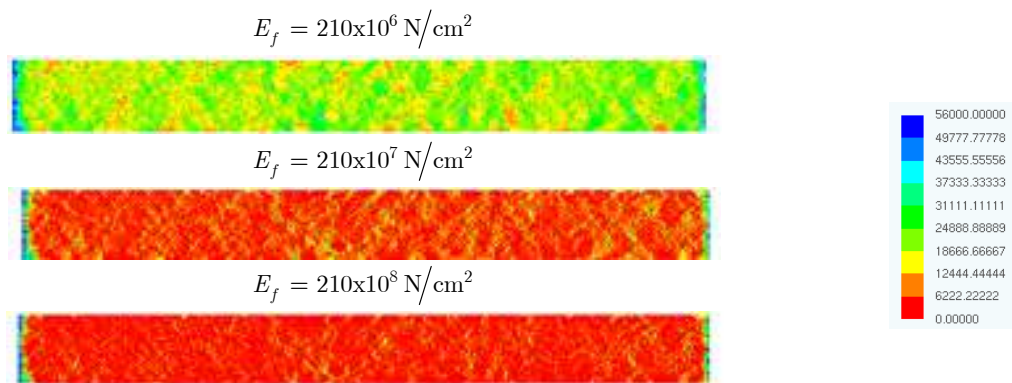


Figure 30: Matrix stress (σ_{11}) distribution – same scale - N/cm^2 .

As the reinforcement elastic modulus grows the average matrix stress reduces. It is obvious that at the extremities of reinforcements localized high stress appears, as depicted in Figure 31.

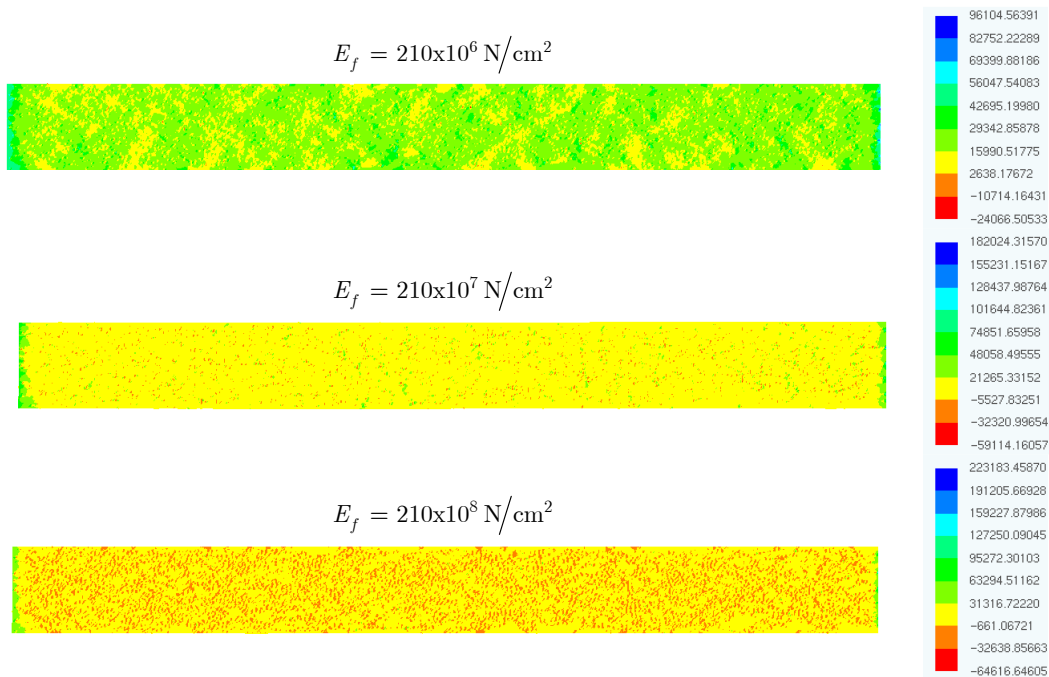


Figure 31: Matrix stress (σ_{11}) distribution – different scale - N/cm^2

7 CONCLUSIONS

In this study an alternative methodology to analyze elastic reinforced solids, fiber matrix coupling, including the calculation of contact stresses is proposed. The procedure is applied in 2D domains and does not increase the number of degrees of freedom of the original 2D mesh. Two methodologies to calculate the contact stress between fiber and matrix are proposed and implemented. The first is applicable to high order fiber elements and is based on differential relations among the reinforcement (or fiber) internal normal stress and the contact stresses, tangential and normal. The other methodology is based on the division of the internal transfer force by a contact influence area. The last is also applicable to straight linear fiber elements.

From the examples we conclude that the overall displacement behavior is almost insensible to both order and number of the adopted fiber finite element discretization. However, an unexpected surprise reveals that the contact stresses for high order elements present spurious behavior for both average and differential calculations. Moreover no convergence is achieved if the number of fiber elements is increased. We concluded that this unexpected and undesirable behavior is due, though hidden, to the improper application of concentrated forces on intermediate node of high order finite elements used to discretize reinforcements. The application of random short fibers is also successfully tested.

In future works we intend to apply the successful developments of this paper to consider slip among fiber and matrix without increasing the number of degrees of freedom.

Acknowledgements

This research is supported by the Coordenação de Aperfeiçoamento de Pessoal de Nível Superior (CAPES), Amazon Research Foundation (FAPEAM) and São Paulo Research Foundation (FAPESP).

References

- Babuska, I., Melenk, J.M., (1997). The partition of unity method. *International Journal for Numerical Methods in Engineering* 40: 727–758.
- Balakrishnan, S., Murray, D.W., (1986). Finite element prediction of reinforced concrete. Ph.D. Thesis, University of Alberta.
- Bolander Jr, J.E., Saito, S., (1997). Discrete modeling of short-fiber reinforcement in cementitious composites. *Advanced Cement Based Materials* 6: 76–86.
- Bonet, J., Wood, R.D., Mahaney, J., Heywood, P., (2000). Finite element analysis of air supported membrane structures. *Computer Methods in Applied Mechanics and Engineering* 5-7: 579-595.
- Ciarlet, P. G., (1993). *Mathematical Elasticity*. North-Holland.
- Chudoba, R., Jerábek, J., Peiffer, F., (2009). Crack-centered enrichment for debonding in two-phase composite applied to textile reinforced concrete. *International Journal for Multiscale Computational Engineering* 7(4): 309–328.
- Coda, H. B., (2001). Dynamic and static non-linear analysis of reinforced media: a BEM/FEM coupling approach. *Computers & Structures*, 79(31): 2751-2765.
- Coda, H.B., (2009). A solid-like FEM for geometrically non-linear 3D frames, *Computer methods in applied mechanics and engineering* 198(47-48): 3712-3722.
- Coda, H.B., Paccola, R.R., (2007). An alternative positional FEM formulation for geometrically nonlinear analysis of shells: Curved triangular isoparametric elements. *Computational Mechanics* 40(1): 185-200.
- Coda, H.B., Paccola, R.R., (2008). A positional FEM Formulation for geometrical non-linear analysis of shells, *Latin American Journal of Solids and Structures* 5(3): 205-223.
- Désir, J.-M., Romdhane, M.R.B., Ulm, F.-J., Fairbairn, E.M.R., (1999). Steel–concrete interface: revisiting constitutive and numerical modeling. *Computers and Structures* 71: 489–503.
- Duarte, C.A., Babuska, I., Oden, J.T., (2000). Generalized finite element methods for three-dimensional structural mechanics problems. *Computers and Structures* 77: 215–232.
- Duarte, C.A., Oden, J.T., (1996a). H-p clouds-an h-p meshless method. *Numerical Methods for Partial Differential Equations* 12: 673–705.
- Duarte C.A., Oden, J.T., (1996b). An h-p adaptive method using clouds. *Computer Methods in Applied Mechanics and Engineering* 139: 237–262.
- Hettich, T., Hund, A., Ramm, E., (2008). Modeling of failure in composites by X-FEM and level sets within a multiscale framework. *Computer Methods in Applied Mechanics and Engineering* 197: 414-424.
- Leite, L.G.S., Venturini, W.S., Coda, H.B., (2003). Two dimensional solids reinforced by thin bars using the boundary element method. *Engineering Analysis with Boundary Elements* 3(27): 193-201.
- Li, Z., Perez Lara, M.A., Bolander, J.E., (2006). Restraining effects of fibers during non-uniform drying of cement composites. *Cement and Concrete Research* 36: 1643–1652.
- Luenberger, D. G., (1989). *Linear and nonlinear programming*. Addison-Wesley Publishing Company.

- Melenk, J.M., Babuska, I., (2006). The partition of unity finite element method: basic theory and applications. *Computer Methods in Applied Mechanics and Engineering* 139: 289–314.
- Oden, J.T., Duarte, C.A.M., Zienkiewicz, O.C., (1998). A new cloud-based hp finite element method. *Computer Methods in Applied Mechanics and Engineering* 153: 117–126.
- Ogden, R.W., (1984). *Nonlinear Elastic deformation*, Ellis Horwood, England.
- Oliver, J., Linero, D.L., Huespe, A.E., Manzoli, O.L., (2008). Two-dimensional modeling of material failure in reinforced concrete by means of a continuum strong discontinuity approach. *Computer Methods in Applied Mechanics and Engineering* 197: 332–348.
- Pascon, J.P., Coda, H.B., (2013). A shell finite element formulation to analyze highly deformable rubber-like materials. *Latin American Journal of Solids and Structures* 10: 1177-1209.
- Radtke, F.K.F., Simone, A., Sluys, L.J., (2010a). A partition of unity finite element method for obtaining elastic properties of continua with embedded thin fibres, *International Journal for Numerical Methods in Engineering* 84 (6): 708-732.
- Radtke, F.K.F., Simone, A., Sluys, L.J., (2010b). A computational model for failure analysis of fibre reinforced concrete with discrete treatment of fibres. *Engineering Fracture Mechanics* 77(4): 597-620.
- Radtke, F.K.F., Simone, A., Sluys, L.J., (2011). A partition of unity finite element method for simulating nonlinear debonding and matrix failure in thin fibre composites. *International Journal for Numerical Methods in Engineering* 86(4-5): 453-476.
- Sampaio, M.S.M., Paccola, R.R., Coda, H.B., (2013). Fully adherent fiber-matrix FEM formulation for geometrically nonlinear 2D solid analysis. *Finite Elements Analysis and Design* 66: 12-25.
- Schlangen, E., Van Mier, J.G.M., (1992). Simple lattice model for numerical simulation of fracture of concrete materials and structures. *Materials and Structures* 25: 534–542.
- Tauchert, T.R., (1974). *Energy principles in structural mechanics*. McGraw Hill.
- Vanalli, L., Paccola, R.R., Coda, H.B., (2008). A simple way to introduce fibers into FEM models. *Communication in numerical methods in Engineering* 24: 585-603.